Cyclic Interconversion among Molecular Salts via Neat Grinding and Related Photoluminescence Properties

Hong-liang Liu,[†] Yi-Fei Xie,[†] Zhi-gang Pan,[‡] Antonino Famulari,[§] Fang Guo,*[,†] Zhongfu Zhou,[∥] and Javier Martí-Rujas*[,⊥]

[†]College of Chemistry, Liaoning University, Shenyang 110036, China

[‡]College of Materials Science and Engineering, Nanjing Tech University, Nanjing 211816, China

[§]Dipartimento di Chimica Materiali e Ingegneria Chimica, "'Giulio Natta"', Politecnico di Milano, Via L. Mancinelli 7, 20131 Milan, Italy

[∥]Key Laboratory for Material Microstructures, Shanghai University, Shanghai 200444, China

[⊥]Center for Nano Science and Technology@Polimi, Istituto Italiano di Tecnologia, Via Pascoli 70/3, 20133 Milano, Italy

■ INTRODUCTION

The dynamic behavior and reactivity of crystalline materials[1−5] is an intriguing research field that allows studying chemical reactions that in the solution state are not accessible. Solid-state reactions induced by gas,[6−12] light,[13−17] or heat[18−22] have provided products that are otherwise very difficult or impossible to produce.

Solid-state mechanochemical synthesis,[23−26] where chemical reactions are carried out by manual grinding or ball milling, is becoming an effective and environmentally friendly synthetic method. It has been successfully applied in many research areas, such as supramolecular synthesis of hydrogen- or halogen-bonded materials,[27−29] clusters and polymers,[30−36] metallodrugs,[37−39] and porous metal−organic frameworks.[40−43] Real-time and *in situ* monitoring of mechanochemical milling reactions has also triggered considerable attention.[44]

Solid-state interconversion, where one cocrystal can transform into a new stoichiometric complex and vice versa by adding/removing molar amounts of one of the starting co-crystallizing components can lead to new solids that in solution are not easy to obtain. However, there are only a few reports on the reversible solid-state ionic mechanochemical interconversion of cocrystals and molecular salts with different stoichiometries until today. The process is intriguing as it provides a way to understand hydrogen bonding rearrangements and relative stabilities between different stoichiometric forms. Mechanochemical interconversion has been used to screen stoichiometric variations of cocrystals using the pharmaceutical compound nicotinamide and 10 dicarboxylic acids.[45] Defined as a sort of supramolecular metathesis, the interconversion between pyrazine and tartaric acid in different isomeric forms was investigated.[46] Also the mechanical interconversion has been used to study the polymorphic transformation of pamoic acid and 1,4-diazabicyclo[2.2.2]-octane (DABCO) cocrystals.[47] Recently, synthon modularity has been proposed as the mechanism of conversion involving

Received: September 24, 2014
Revised: October 31, 2014
Published: November 7, 2014

hydroxybenzoic acids with hexamine, corroborated by theoretical calculations.[48]

Most of the reported mechanochemical interconversion reactions are carried out via liquid assisted grinding (LAG),[49] while neat grinding is less commonly used as it often fails to give the desired product and gives products with a lower degree of crystallinity.[45] We have described a reversible solid-state ionic interconversion between two stoichiometric forms (1:1 and 1:2) of hydrogen bonded molecular salts upon neat grinding by adding 1 equiv of one of the components.[50] The system involved 5-sulfosalicilic acid dihydrate and the amphoteric base benzimidazole. The results were supported by quantum mechanics calculations specific for solid-state systems.[51] To our best knowledge, studies involving interconversion and their photoluminescent properties of molecular salts with three stoichiometirc forms using neat grinding are still unusual.

Herein, we have cocrystallized three new molecular salts $\mathbf{A_1B_1{\cdot}H_2O}$, $\mathbf{A_1B_2}$ and $\mathbf{A_2B_1}$ and used the molecular salt $\mathbf{A_2B_1{\cdot}H_2O}$[52] (where $\mathbf{A{\cdot}2H_2O}$ = 5-sulfosalicilic acid dihydrate and **B** = 4,4′-diaminodiphenylmethane) to study their reversible solid state ionic interconversion by neat grinding. The salts $\mathbf{A_1B_1{\cdot}H_2O}$, $\mathbf{A_1B_2}$, and $\mathbf{A_2B_1{\cdot}H_2O}$ can be interconverted by adding the appropriate amount of one of the corresponding cocrystallizing components ($\mathbf{A{\cdot}2H_2O}$ or **B**) upon grinding (Scheme 1). The

Scheme 1. Synthesis and Interconversion between $\mathbf{A_1B_1{\cdot}H_2O}$, $\mathbf{A_1B_2}$, and $\mathbf{A_2B_1{\cdot}H_2O}$ Applying Neat Grinding

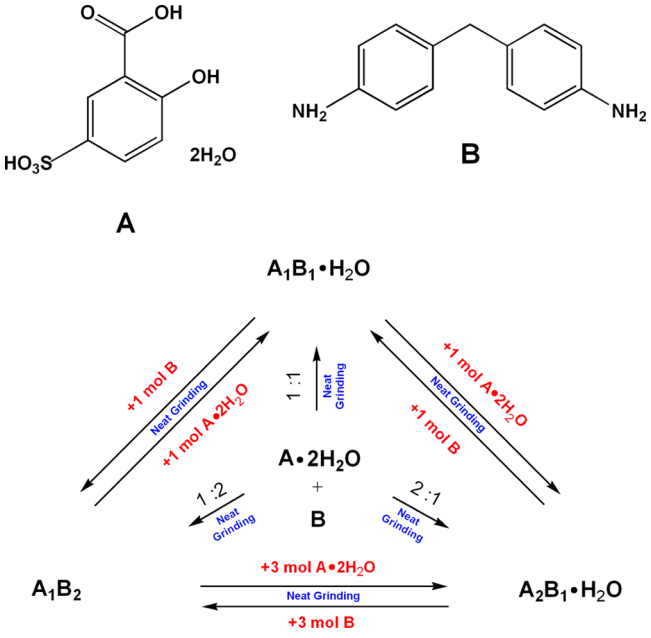

amount of water present in $\mathbf{A{\cdot}2H_2O}$, $\mathbf{A_1B_1{\cdot}H_2O}$, or $\mathbf{A_2B_1{\cdot}H_2O}$ is comparable with that typically used for LAG, suggesting its "catalytic" role as a proton shuttle in the mechanochemical transformation. The solid-state photoluminescence properties of the cocrystallizing components and that of the molecular salts $\mathbf{A_1B_1{\cdot}H_2O}$, $\mathbf{A_1B_2}$, and $\mathbf{A_2B_1{\cdot}H_2O}$ are reported. The experimental results are corroborated with time-dependent density functional theory (TD−DFT) calculations, demonstrating the contribution of the anions of **A** on the emissive properties in this family of molecular salts.

EXPERIMENTAL SECTION

Synthesis and Crystal growth. *Solution.* $\mathbf{A{\cdot}2H_2O}$ and **B** were weighed in 1:1 and 1:2 molar ratios and dissolved in EtOH, producing large single crystals of salts $\mathbf{A_1B_1{\cdot}H_2O}$ and $\mathbf{A_1B_2}$, respectively. $\mathbf{A{\cdot}2H_2O}$ and **B** were weighed in 2:1 molar ratios and dissolved in EtOH, producing large transparent single crystals of $\mathbf{A_2B_1}$.

Solid State Grinding. $\mathbf{A{\cdot}2H_2O}$ and **B** were mixed in appropriate stoichiometries (e.g., 1:1, 1:2, and 2:1) and then coground in a mortar and pestle for 10 min, forming $\mathbf{A_1B_1{\cdot}H_2O}$, $\mathbf{A_1B_2}$ and $\mathbf{A_2B_1{\cdot}H_2O}$.

Solid-State Fluorescence. Solid-state fluorescence spectra were obtained with a Hitachi Fluorescence spectrophotometer F-7000 measured at room temperature. The excitation wavelength used was 350 nm.

Crystallography. Single crystal data collection was performed with Mo Kα radiation (λ = 0.71073 Å) on a Bruker P4 diffractometer. Powder X-ray diffraction was recorded at room temperature on a D8 Bruker diffractometer (λ = 1.54056 Å), with Cu Kα-radiation and a step size of 0.01°.

Single Crystal Data for $\mathbf{A_1B_1{\cdot}H_2O}$. $C_7H_4O_6S^{2-}{\cdot}C_{13}H_{16}N_2^{2+}{\cdot}H_2O$, M_r = 434.47, crystal dimensions 0.228 × 0.041 × 0.040 mm^3, monoclinic, space group, $P2_1/c$, unit cell, a = 6.1214 (12) Å, b = 17.328(3) Å, c = 19.009(4) Å; β = 96.294(3)°, V = 2004.2(7) Å^3, T = 296(2) K, Z = 4. Anisotropic least-squares refinement (304 parameters) on 4561 independent merged reflections (R_{int} = 0.0443) converged at $wR_2(|F|^2)$ = 0.1238 for all data; $R_1(F)$ = 0.0470 for 2748 observed data ($I > 2(I)$), GOF = 1.046. CCDC number: 1021217.

Single Crystal Data for $\mathbf{A_1B_2}$. $C_7H_4O_6S^{2-}{\cdot}2C_{13}H_{15}N_2^{+}$, M_r = 614.7, crystal dimensions 0.280 × 0.250 × 0.120 mm^3, monoclinic, space group, $P2_1/c$, unit cell, a = 13.692(13) Å, b = 10.075(10) Å, c = 22.69(2) Å; β = 102.745(11)°, V = 3052(5) Å^3, T = 296 (2) K, Z = 4. Anisotropic least-squares refinement (407 parameters) on 6936 independent merged reflections (R_{int} = 0.0230) converged at $wR_2(|F|^2)$ = 0.1151 for all data; $R_1(F)$ = 0.0409 for 5261 observed data ($I > 2(I)$), GOF = 1.030. CCDC number: 1021218.

Single Crystal Data for $\mathbf{A_2B_1}$. $2C_7H_5O_6S^{-}{\cdot}C_{13}H_{16}N_2^{2+}$, M_r = 634.62, crystal dimensions 0.280 × 0.200 × 0.140 mm^3, monoclinic, space group, $P2_1/c$, unit cell, a = 12.676(4) Å, b = 17.643(5) Å, c = 13.575(4) Å; β = 114.989(3)°, V = 2751.6(15) Å^3, T = 296(2) K, Z = 4. Anisotropic least-squares refinement (492 parameters) on 6323 independent merged reflections (R_{int} = 0.0222) converged at $wR_2(|F|^2)$ = 0.1002 for all data; $R_1(F)$ = 0.0373 for 5076 observed data ($I > 2(I)$), GOF = 1.030. CCDC number: 1021219.

RESULTS AND DISCUSSION

Structure of 5-Sulfonatosalicylate 4,4′-Diaminodiphenylmethane Monohydrate Salt ($\mathbf{A_1B_1{\cdot}H_2O}$). The molecular salt $\mathbf{A_1B_1{\cdot}H_2O}$ was prepared by mixing 0.048 mmol of $\mathbf{A{\cdot}2H_2O}$ and 0.048 mmol of **B**. X-ray powder diffraction (XRPD) analysis confirmed that product $\mathbf{A_1B_1{\cdot}H_2O}$ obtained from solution and grinding is the same (Figure S1, Supporting Information). In $\mathbf{A_1B_1{\cdot}H_2O}$, the asymmetric unit contains one **A** dianion, one **B** dication, and one water molecule. As shown by single crystal X-ray analysis, there is proton transfer from the carboxyl and sulfonate groups of **A** to two amine groups of **B**.[53] We note that while the monoanionic species are quite common with Lewis bases, the formation of the 5-sulfonatosalicylate dianion is less common.[54]

All functional groups of **A** and **B** molecules are engaged in hydrogen bonding interactions (Figure 1, Figure S4, Table S2). The hydroxyl and the carboxyl groups of **A** dianion form the intramolecular interaction (i). One NH_3^+ group (N2) in **B** cation forms three hydrogen bonds with O4 and O6 on the SO_3 group in one **A** dianion (ii), (iii) and O3 of carbonyl group in another **A** dianion (iv). The other NH_3^+ group (N1) also forms three hydrogen bonds, linking with O5 of SO_3 in one **A** dianion (v), O2 of carboxyl group in another **A** dianion (vi)

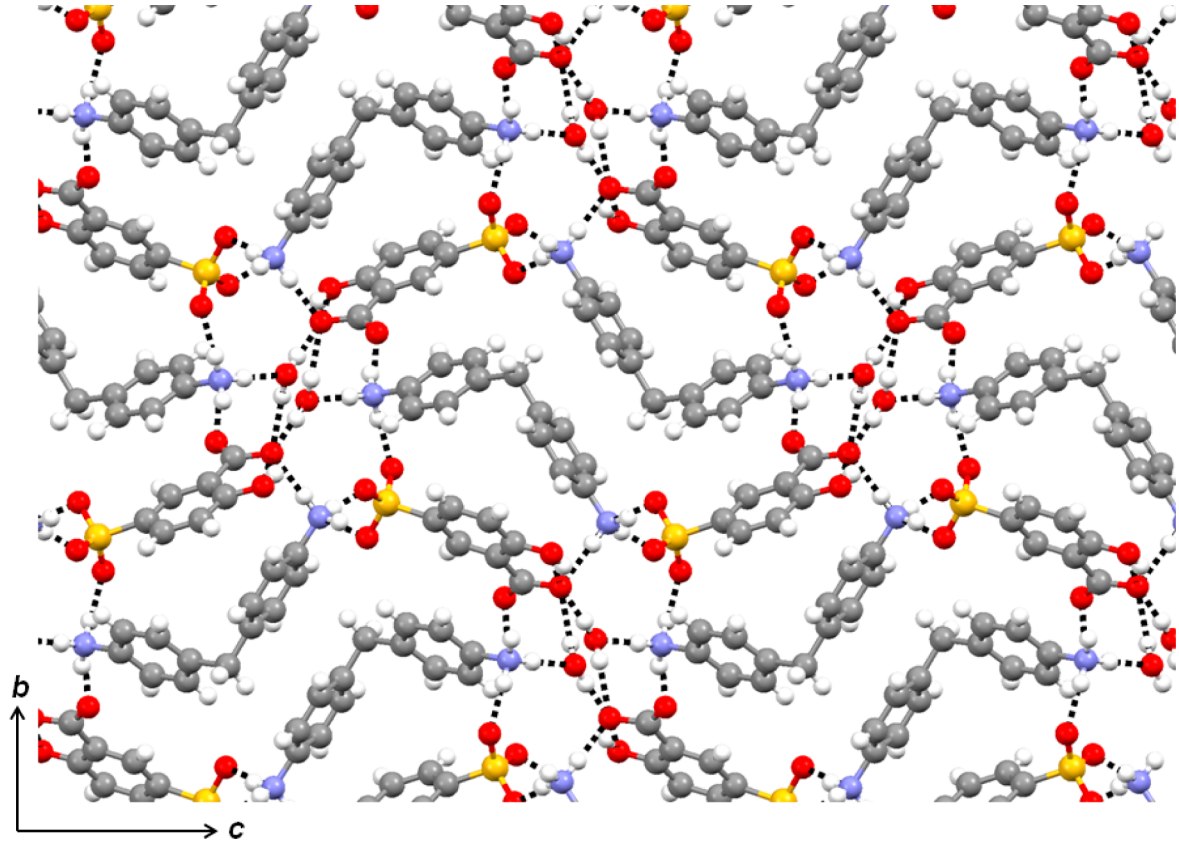

Figure 1. Crystal structure of $A_1B_1 \cdot H_2O$ viewed along the *a*-axis. Hydrogen bonds are shown as black dash lines. Color code: carbon (gray); nitrogen (blue); oxygen (red); sulfur (yellow); hydrogen (white).

and water molecule (vii). Each water molecule, as hydrogen bond donor, is connecting with two O atoms of the carboxyl groups (viii) while receiving as acceptor (vii). In the crystal packing, loose $\pi-\pi$ interactions (4.016 Å) between **A** cations are observed.

Despite the fact that we have used 5-sulfosalicilic acid dihydrate to crystallize with 4,4′-diaminodiphenylmethane, and the good ability of water to establish HB interactions, the salt precipitated as a monohydrate phase. Therefore, one water molecule in $A \cdot 2H_2O$ is excluded in the final structure.

Structure of the 5-Sulfonatosalicylate Bis(4,4′-diaminodiphenylmethane) Salt (A_1B_2). The mechanochemical synthesis of A_1B_2 was carried out by mixing **A** and **B** in a 1:2 molar ratio (0.048:0.096 mmol respectively) and grinding the mixture for 10 min. The good match between the experimental XRPD obtained after grinding **A** and **B**, and the simulated diffraction pattern from single crystal corroborates that the bulk product corresponds to A_1B_2 (Figure S2, Supporting Information). The molecular salt A_1B_2 contains one **A** dianion and two independent **B** cations in the asymmetric unit. The two protons in the carboxylic and sulfonate groups of **A** anions have been transferred to one NH_2 group of the two independent **B** cations (Figure S5). The **B** molecule in A_1B_2 structure is monoprotonated. Detailed hydrogen bond interactions are shown in Table S3. The intramolecular hydrogen bonding (i) between the carbonyl and carboxyl groups in **A** molecule is maintained. The overall structure of A_1B_2 can be regarded as layered, in which the layers formed by **B** cations are sandwiched between the layers formed by **A** dianions (Figure 2) with an arrangement of perpendicular to each other.

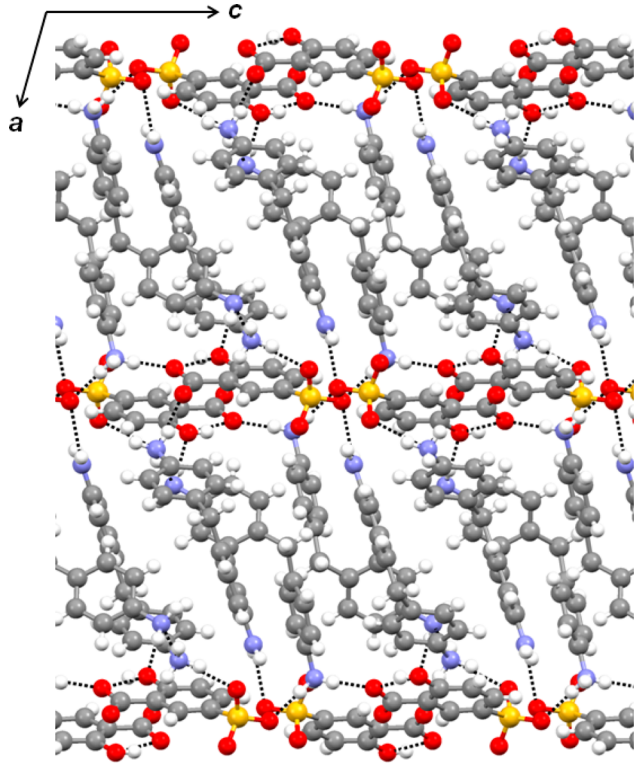

Figure 2. Single crystal structure of A_1B_2 viewed along the *b*-axis. Hydrogen bonds are shown as black dash lines. Color coded as in Figure 1.

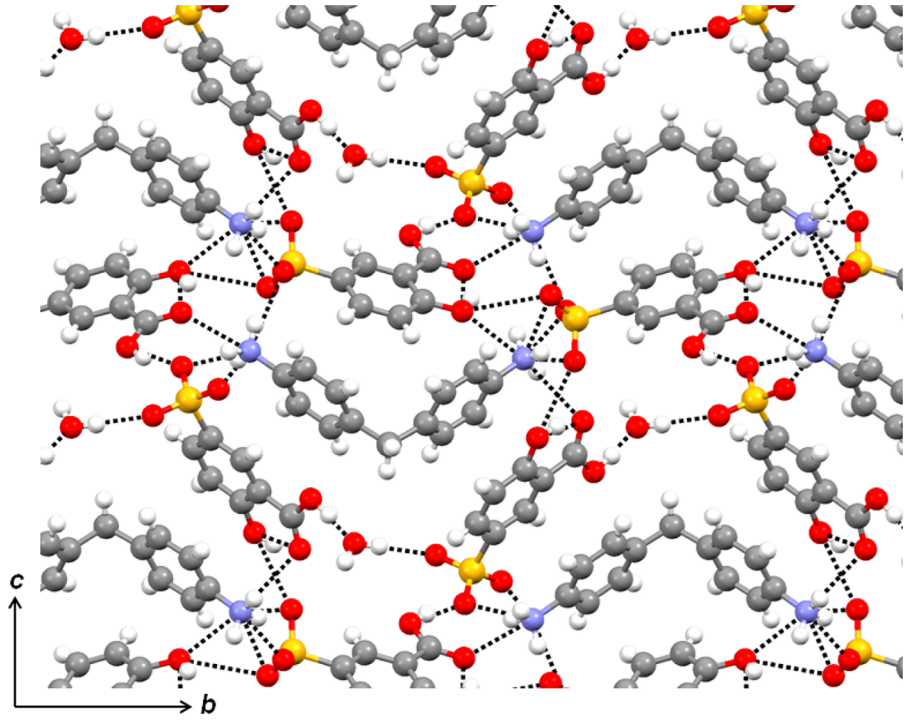

Figure 3. Synthesis Single crystal structure of $A_2B_1 \cdot H_2O$ viewed along the *a*-axis. Hydrogen bonds are shown in dashed lines. Color coded as in Figure 1.

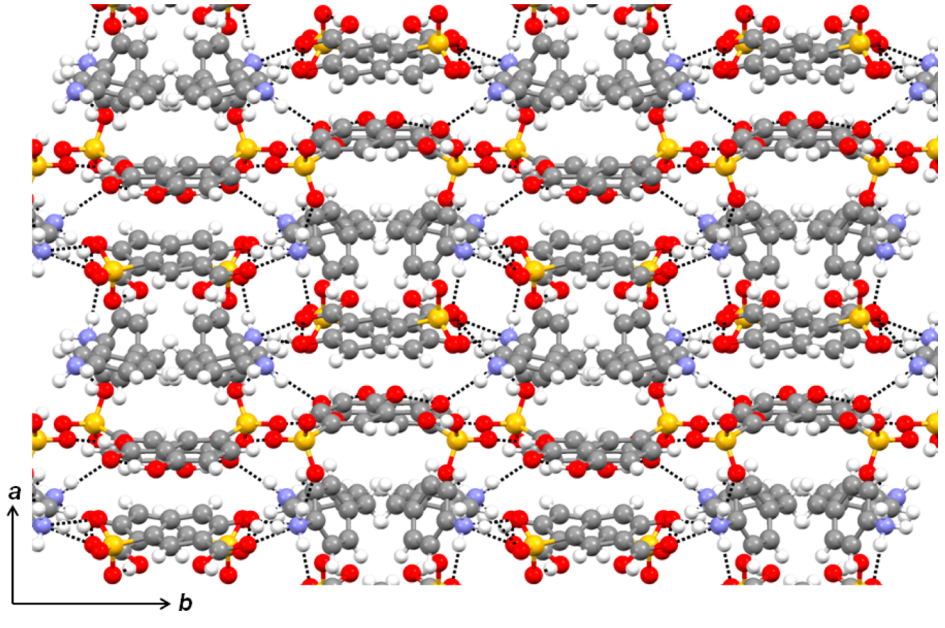

Figure 4. Single crystal structure of A_2B_1 viewed along the *c*-axis. Hydrogen bonds are shown in dashed lines. Color coded as in Figure 1.

The connection between the cationic and anionic layers is through extensive hydrogen bonds (ii−ix) between the functional groups of **A** and **B** (Figure 2, Figure S5 and Table S3). In one independent **B** cation, the NH_3^+ group (N1) is hydrogen bonded to O3 of carboxyl group (ii) and O6 of sulfonate group (iii) of **A** anion and NH_2 group of another cation (iv). In the other independent **B** cation, the NH_3^+ group (N3) is hydrogen bonded to the O2 of carboxyl group (v), the O4 and the O5 of sulfonate group (vi, vii) of the **A** anion. Additionally, the unprotonated NH_2 groups in two independent cations are also involved into the hydrogen bonds: one NH_2 group is connected with the hydroxyl group O1 of **A** anion (viii), the other NH_2 group is linked to O4 of the SO_3 group (ix). Meanwhile there are $\pi-\pi$ interactions (3.792 Å) between **A** and **B** ions.

Structures of Bis(5-sulfosalicylate) 4,4′-Diaminodiphenylmethane Monohydrate Salt $A_2B_1 \cdot H_2O$ and Its Anhydrous Salt (A_2B_1). $A \cdot 2H_2O$ and **B** were weighed in 2:1 molar ratios (0.124:0.062 mmol respectively) and dissolved in ethanol. The phase purity was corrobotated by XRPD (Figure S3). Numerous attempts mostly resulted in the crystallization of $A_1B_1 \cdot H_2O$, and only once we obtained the anhydrous

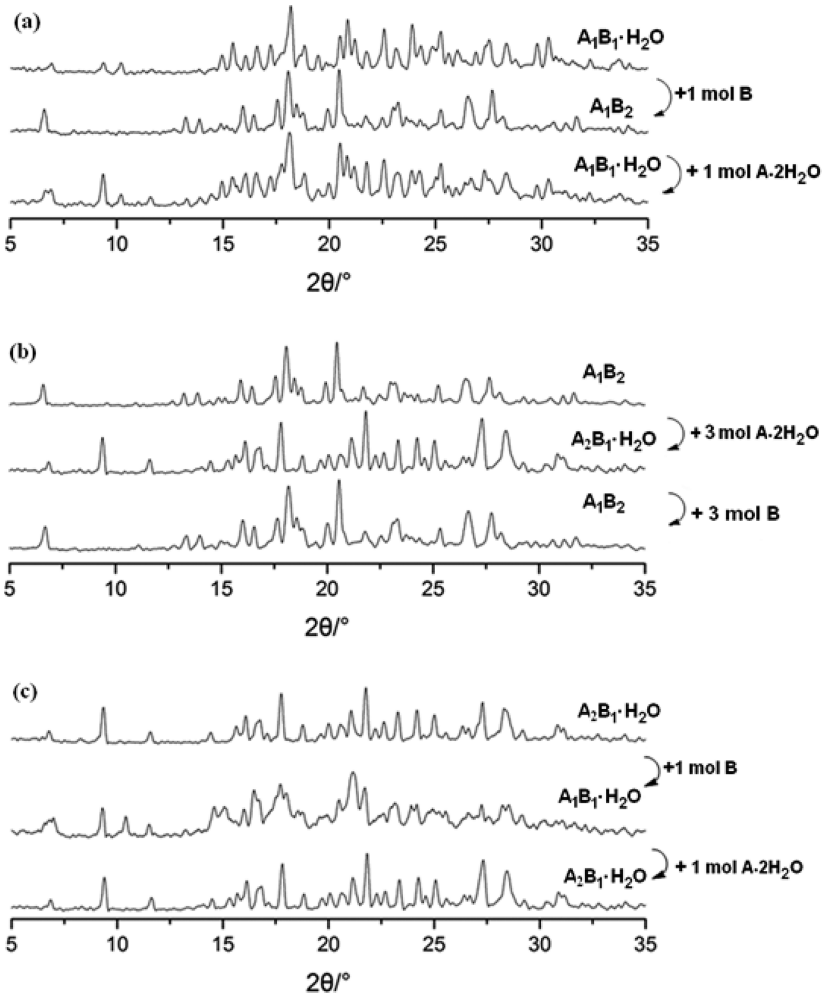

Figure 5. Neat grinding interconversion between $\mathbf{A_1B_1{\cdot}H_2O}$ and $\mathbf{A_1B_2}$ (a), $\mathbf{A_1B_2}$ and $\mathbf{A_2B_1{\cdot}H_2O}$ (b), and $\mathbf{A_2B_1{\cdot}H_2O}$ and $\mathbf{A_1B_1{\cdot}H_2O}$ (c).

molecular salt (vide infra). However, we found that $\mathbf{A_2B_1{\cdot}H_2O}$ was readily obtained by solid state grinding as shown by XRPD (Figure S3) but not $\mathbf{A_2B_1}$.

$\mathbf{A_2B_1{\cdot}H_2O}$ crystallizes in the $P2_1$ space group, while anhydrous $\mathbf{A_2B_1}$ forms crystals belonging to the $P2_1/c$ space group. In both structures, the proton transfer occurs from the sulfonate group of two independent **A** anions to two NH_2 groups of one **B** cation.

In $\mathbf{A_2B_1{\cdot}H_2O}$, there are two independent **A** anions, one cation, and one water molecule (Figure S6 and S7). Detailed hydrogen bond interactions are shown in Table S4. The intramolecular hydrogen bond in **A** is preserved in both molecules (i_a and i_b) as in all the previous structures. The two protonated amino groups form an important hydrogen bond network with **A**. The NH_3^+ group involving N1 interacts with the carboxylic group through O4 (ii) and with the sulfonate group, O11 (iii), O12 (iv) atoms (Figures S6 and S7). The protonated NH_3^+ (N2) interacts with the other independent anion through O4 (v), O5 (vi), and O6 (vii) belonging to the sulfonate group. Also the hydroxyl group (O3) interacts with the NH_3^+ (N2) via a bifurcated hydrogen bond (i and viii). The water molecule (O13) establishes hydrogen bonds with the sulfonate (O10) (ix) and the carboxylic group (O8) (x) of neighboring molecules (Figures S6 and S7). The carboxyl group (O2) also establishes a hydrogen bond with the oxygen of the sulfonate group (O11) (xi). In this molecular salt, $\pi-\pi$ interactions (3.746 Å) between **A** cations are observed.

As shown in Figure S8, in $\mathbf{A_2B_1}$, the intramolecular hydrogen bond in **A** is preserved in both molecules (i_a and i_b) as in all the previous structures. The extensive hydrogen bond interactions involve one of the NH_3^+ groups (N1) that interacts with a sulfonate group via O5 (ii) and O7 (iii), and with the carboxylic group through O8 (iv) hydrogen bonds. The second NH_3^+ group (N2) forms hydrogen bonds with the sulfonate group via O5 (v), O7 (vi), and O2 (vii) hydrogen bonds. Moreover the carboxylic group also interacts through O9 (viii). Furthermore, $\pi-\pi$ stacking (3.576 Å) between two independent **A** anions in $\mathbf{A_2B_1}$ are present. Detailed hydrogen bond interactions are shown in Table S4.

Mechanochemical Interconversion between $\mathbf{A_1B_1{\cdot}H_2O}$, $\mathbf{A_1B_2}$ and $\mathbf{A_2B_1{\cdot}H_2O}$ Molecular Salts in the Solid State. Salts $\mathbf{A_1B_1{\cdot}H_2O}$, $\mathbf{A_1B_2}$, and $\mathbf{A_2B_1{\cdot}H_2O}$ can be mechanochemically interconverted in the solid state by adding an appropriate amount of one of the corresponding crystallizing components ($\mathbf{A{\cdot}2H_2O}$ or **B**). Crystalline $\mathbf{A_1B_1{\cdot}H_2O}$ salt was first prepared by neat grinding (10 min) in a 1:1 molar ratio of $\mathbf{A{\cdot}2H_2O}$ and **B**, and then one mol of **B** was added to $\mathbf{A_1B_1{\cdot}H_2O}$ and further ground for 10 min. XRPD confirmed that $\mathbf{A_1B_2}$ was produced (Figure 5a). Further addition of 1 mol of $\mathbf{A{\cdot}2H_2O}$ to $\mathbf{A_1B_2}$, followed by grinding, resulted in the formation of $\mathbf{A_1B_1{\cdot}H_2O}$. The same interconversion between $\mathbf{A_1B_2}$ and $\mathbf{A_2B_1{\cdot}H_2O}$

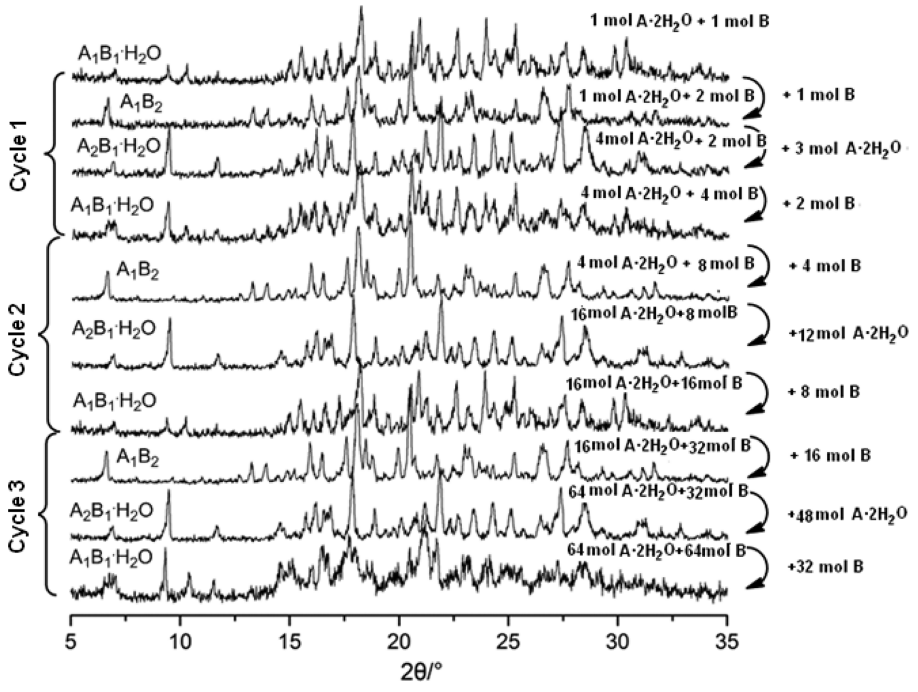

Figure 6. Cyclic mechanochemical interconversion between $\mathbf{A_1B_1{\cdot}H_2O}$, $\mathbf{A_1B_2}$, and $\mathbf{A_2B_1{\cdot}H_2O}$ via neat grinding.

and between $\mathbf{A_2B_1{\cdot}H_2O}$ and $\mathbf{A_1B_1{\cdot}H_2O}$ can also be done as shown by XRPD (Figure 5b,c).

Additionally, the reversible interconversion between the three salts was further confirmed by XRPD by repeating for several cycles the addition of $\mathbf{A{\cdot}2H_2O}$ or **B** in the corresponding ratios. The $\mathbf{A_1B_1{\cdot}H_2O}$ salt was first prepared to which one mol of **B** was added to produce the anhydrous salt $\mathbf{A_1B_2}$. Then, 3 mol of $\mathbf{A{\cdot}2H_2O}$ was added to $\mathbf{A_1B_2}$ and the mixture subsequently ground for 10 min, which gave the hydrated $\mathbf{A_2B_1{\cdot}H_2O}$ salt. Finally, to close the cycle, 2 mol of **B** was added to $\mathbf{A_2B_1{\cdot}H_2O}$ and the mixture was ground for 10 min, producing $\mathbf{A_1B_1{\cdot}H_2O}$ again (Figure 6).

In the conversion from $\mathbf{A_1B_1{\cdot}H_2O}$ to $\mathbf{A_1B_2}$ by adding 1 mol of **B** (i.e., that does not contain water), there is proton transfer from the carboxylic group and the sulfonate group of **A** to the amine groups of **B.** The dicationic species switch to monocationic species. The reverse switch from monocationic to dicationic species can be carried out if 1 mol of $\mathbf{A{\cdot}2H_2O}$ is added to $\mathbf{A_1B_2}$ and the mixture ground. The presence of additional sulfonic groups in the incoming $\mathbf{A{\cdot}2H_2O}$ molecule allows for the structural reorganization and proton transfer, such that the carboxylate group in the reacting $\mathbf{A_1B_2{\cdot}H_2O}$ is restored as carboxylic acid to form $\mathbf{A_1B_1}$. Similarly, there is also change of proton transfer between the $\mathbf{A_1B_1{\cdot}H_2O}$ to $\mathbf{A_2B_1{\cdot}H_2O}$, followed by the switch between monoanionic to dianionic species. Thus, the addition of an extra Lewis acid/base induces the proton transfer in a system where various hydrogen bond donors (i.e., carboxylic and sulfonic acid groups) can react in the solid state.

We note that water molecules are crucial in the solid state reaction, helping the proton transfer process by acting as proton carrier. In fact, the X-ray crystal structure of $\mathbf{A{\cdot}2H_2O}$ shows that proton transfer takes place forming the hydronium cation (H_3O^+) and the 5-sulfosalicylate anion.[55] Hence in the solid state synthesis of salts $\mathbf{A_1B_1{\cdot}H_2O}$ and $\mathbf{A_2B_1{\cdot}H_2O}$ using $\mathbf{A{\cdot}2H_2O}$ and **B**, and the solid state interconversion from $\mathbf{A_1B_2}$ to $\mathbf{A_1B_1{\cdot}H_2O}$ or $\mathbf{A_2B_1{\cdot}H_2O}$, the proton transfer might be water mediated and occurs from H_3O^+ to 4,4′-diaminodiphenylmethane.[56] This demonstrates that water molecules are essential for the reaction (i.e., proton transfer) to occur between the reactants.

Solid-State Photoluminescence of $\mathbf{A{\cdot}2H_2O}$ and B Starting Materials, and the Molecular Salts $\mathbf{A_1B_1{\cdot}H_2O}$, $\mathbf{A_1B_2}$, and $\mathbf{A_2B_1{\cdot}H_2O}$: A Combined Experimental and Molecular Modeling Study. Co-crystallization can promote the optical properties of a given material by combining molecules with functional groups able to establish electrostatic interactions.[57−61] Luminescent adducts are important for applications as chemical sensors and electroluminescent displays. We were interested in studying the photoluminescence (PL) behavior upon the addition of one of the molecular components (i.e., $\mathbf{A{\cdot}2H_2O}$ and **B**) to the $\mathbf{A_1B_1{\cdot}H_2O}$, $\mathbf{A_1B_2}$, and $\mathbf{A_2B_1{\cdot}H_2O}$ molecular salts in the solid-state regarding the effect of the protonation state of the molecular species. Figure 7 illustrates the emission spectra of the three salts and their molecular components $\mathbf{A{\cdot}2H_2O}$ and **B**. The ionic salts are red-shifted compared with the starting materials. The maximum emission of $\mathbf{A{\cdot}2H_2O}$ and **B** is below 400 nm (386 nm for $\mathbf{A{\cdot}2H_2O}$ and 358 nm for **B** respectively), whereas $\mathbf{A_1B_1{\cdot}H_2O}$, $\mathbf{A_1B_2}$, and $\mathbf{A_2B_1{\cdot}H_2O}$ can reach 412, 398, and 441 nm, respectively. We consider that emission from $\mathbf{A_1B_1{\cdot}H_2O}$, $\mathbf{A_1B_2}$, $\mathbf{A_2B_1{\cdot}H_2O}$ molecular salts should be due to charge transfer associated with the starting organic molecules. As they all emit light, we rule out the quenching effect as a result of close packing. However, we do see a considerable difference among them regarding their emission features (Figure 7). As it is known that in the solid-state π-stacked structures tend to suppress PL properties, we find that $\mathbf{A_2B_1{\cdot}H_2O}$ has much higher PL despite having a better $\pi-\pi$ interaction among anions (3.746 Å). A similar trend is also observed in the $\pi-\pi$ interaction among **A** and **B** in $\mathbf{A_1B_2}$ (3.792 Å) when compared to the $\pi-\pi$ interaction between **A** anions in $\mathbf{A_1B_1{\cdot}H_2O}$ (4.016 Å).

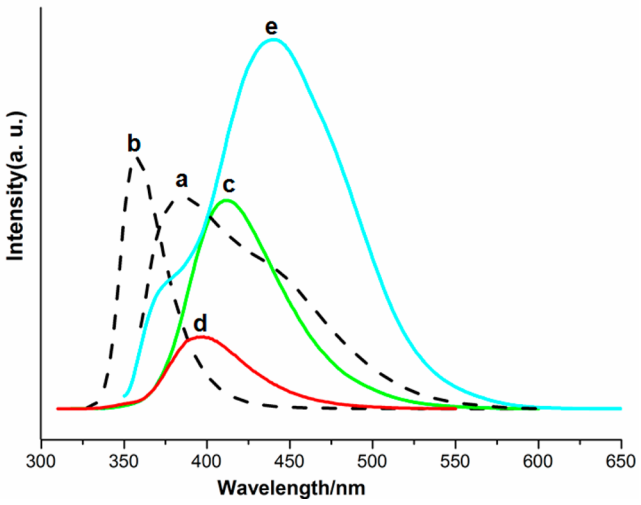

Figure 7. Solid-state fluorescence emissions: a: **A·2H$_2$O**; b: **B** (dash lines); c: **A$_1$B$_1$·H$_2$O**; d: **A$_1$B$_2$**; e: **A$_2$B$_1$·H$_2$O** (solid lines).

Another reason for the different emissive behaviors among **A$_1$B$_1$·H$_2$O**, **A$_1$B$_2$**, and **A$_2$B$_1$·H$_2$O** salts might be related to the proton transfer from **A** to **B**. It seems that when the acid is doubly deprotonated (i.e., involving the protons from the sulfonic and carboxylic groups) the fluorescence intensity is lower (Figure 7). However, the higher wavelength is observed in **A$_2$B$_1$·H$_2$O**, in which each acid molecule is only mono-deprotonated. This trend has also been observed in other molecular salts.[62]

In order to rationalize the observed PL spectra, the energies of electronic excited states of the species involved in the crystalline phases under investigation are necessary. In particular, single excitations from the ground state of the system need to be evaluated to estimate vertical transition energies. The latter are the difference between excited states and ground states energies on a given geometry, which is generally the ground state geometry.

First of all we observe that in all crystalline phases we have the species **A** in an anionic form (**A**$^-$ and **A**$^{2-}$), while **B** is a neutral molecule in **B** or a cation (**B**$^+$ or **B**$^{2+}$) in all the other cases. Since an anion is generally more polarizable than a neutral or a cationic species,[63] we expect that, approximately, the lower excitation energies in such molecular salts are related to electronic states involving mainly energy levels of **A** than that of **B**. This is confirmed by a first glance observing the PL spectra of Figure 7, where the maximum concerning energy levels of species **B** in its pristine crystalline form is blue-shifted with respect to all the other emission profiles.

To confirm the above qualitative considerations and to justify the observed PL spectra, calculations on excited states of species involved into the crystalline phases have been carried out. The extension of DFT to the time-dependent domain is employed, namely, TD-DFT, which is known to provide reasonable results for the excited states of molecules.[64−67] The input geometries of all the fragments were first optimized as isolated molecules and then arranged in small clusters (dimers, trimers, and tetramers) conforming the crystal packing, (i.e., preserving the relative positions and orientations). The B3LYP functional was adopted together with the 6-31G** basis set as implemented in the suite of programs GAUSSIAN09,[68] used for all TD-DFT calculations (see details in Supporting Information). The outcomes demonstrated a semiquantitative consistency with the available experimental data.

To begin with, in the case of **B** neutral molecule the estimated emission maximum is at 4.74 eV corresponding to a wavelength of 261 nm. The calculated wavelength increases improving the agreement with the experimental values by considering in the calculations dimers, trimers, and tetramers extracted from the **B** crystal structure (i.e., in the case of the tetramer the wavelength is 286 nm). Considering **B**$^+$ and **B**$^{2+}$ cations, the estimated energy gap between ground and first excited state increases, while the wavelength decreases. In the case of **B**$^{2+}$ we have in fact 5.46 eV corresponding to 227 nm so that we can confirm that in the molecular salts under study, the

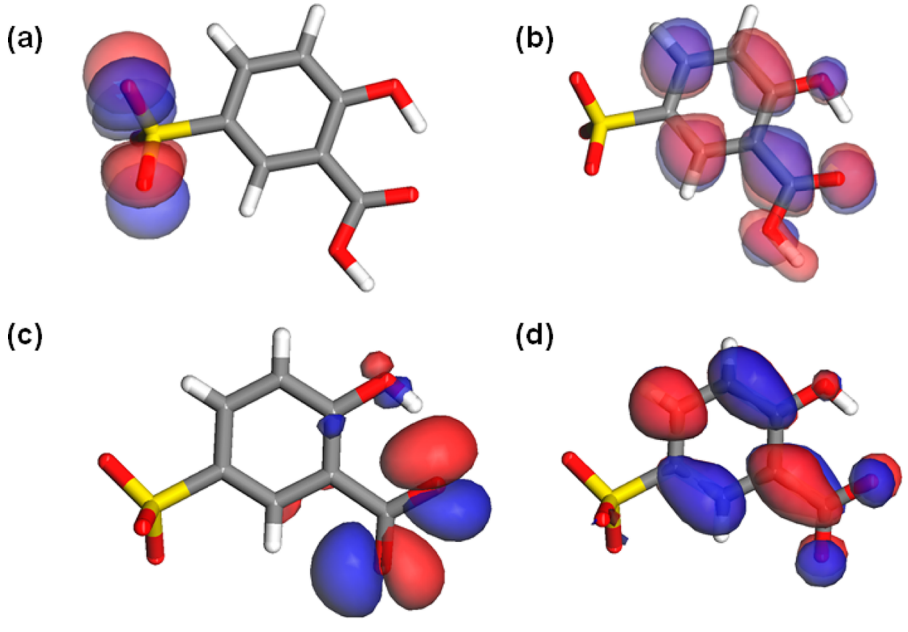

Figure 8. HOMO (a, c) and LUMO (b, d) orbitals involved in the emission of **A**$^-$ **and A**$^{2-}$. Color codes as in Figure 1.

excited energy levels of **B** are to a first approximation marginally involved.

Regarding **A** species and its molecular salts, we first calculated the emission maximum of the monodeprotonated anion (A^-) appearing in both $A{\cdot}2H_2O$ and $A_2B_1{\cdot}H_2O$ compounds. The calculated emission for an isolated anion is 473 nm in wavelength to be compared with the experimental values of 386 and 441 nm for $A{\cdot}2H_2O$ and $A_2B_1{\cdot}H_2O$, respectively. In order to give a very simple picture of these outcomes, in Figure 8a,b we report the HOMO and LUMO orbitals of A^-: the HOMO orbital is condensed at the SO_3^- moiety, while the LUMO orbital delocalizes to the other side of the molecule allowing a direct influence on the PL spectra by interparticle interactions in the molecular salts. In fact, when even a small cluster such as $A^-\cdots H_3O^+H_2O$ (extracted from $A{\cdot}2H_2O$ crystal structure) is considered, due to the strong interaction of close packed H_3O^+ with the SO_3^- group, the corresponding calculated emission maximum readily blue-shifts to 3.58 eV corresponding to 346 nm, which is in semi-quantitative agreement with the experimental value of 386 nm observed in $A{\cdot}2H_2O$. Because of the high steric hindrance, the effects corresponding to the bulkier cations of **B** species are lighter.

In the case of the doubly deprotonated A^{2-} anion, involved in molecular salts A_1B_2 and $A_1B_1{\cdot}H_2O$, we calculated an emission maxima of 3.89 eV corresponding to 319 nm, which differs considerably from that of A^- (473 nm). As shown in Figure 8c,d, the HOMO orbital of A^{2-} species localizes at the COO^- group instead of SO_3^-. In this case the strong interaction of A^{2-} with the dication B^{2+} in $A_1B_1{\cdot}H_2O$ red-shifts the emission maximum to 2.71 eV corresponding to 458 nm, while in the case of A_1B_2 the effect is milder because of the mono cation B^+, in qualitative agreement with the experimental results.

In conclusion, we showed the influence of the charges of anions and cations in the PL spectra and the importance of their molar ratio. Even if the emissive properties concerns complex inter- and intramolecular interactions, qualitatively we can assume that the presence of an extra anion, with the same cation, really affects the emissive properties ongoing from the molecular salt $A_1B_1{\cdot}H_2O$ to $A_2B_1{\cdot}H_2O$. This is a clear example on how the PL properties of molecular salts can be tuned with the addition or release of one of the molecular components.

CONCLUSIONS

We have reported the single crystal X-ray structures of three new molecular salts formed by 5-sulfosalicilic acid dihydrate and 4,4′-diaminodiphenylmethane using 1:1, 1:2, and 2:1 molar ratios. The molecular salts are self-assembled via charge-assisted and neutral hydrogen bonding interactions. The acid−base proton transfer has been readily observed by single crystal X-ray diffraction. We described the reversible solid state ionic interconversion among $A_1B_1{\cdot}H_2O$, A_1B_2, and $A_2B_1{\cdot}H_2O$ upon neat grinding by adding an appropriate amount of $A{\cdot}2H_2O$ or **B**. In the process water molecules are included or excluded upon grinding suggesting that water mediates the proton transfer. The solid-state fluorescence spectra showed that $A_1B_1{\cdot}H_2O$, A_1B_2, $A_2B_1{\cdot}H_2O$ molecular salts all exhibit emission features and have red-shifts compared to the starting materials $A{\cdot}2H_2O$ and **B**. Using TD−DFT calculations, we have demonstrated the contribution of the anions in the fluorescence emission and the influence of the related cations. The frontier molecular orbitals and the energy levels of anions showed a primary role in a semiquantitative comparison with the experiments, mainly due to the higher polarizability of the anions with respect to the cations. The established interparticle (CT) interactions and the degree of anion deprotonation are very important in the solid-sate fluorescence of the described molecular salts.

ASSOCIATED CONTENT

Supporting Information

Further details on the synthesis and crystallographic information. This material is available free of charge via the Internet at http://pubs.acs.org.

AUTHOR INFORMATION

Corresponding Authors

*(F.G.) E-mail: fguo@lnu.edu.cn.

*(J.M.-R.) E-mail: javier.rujas@iit.it.

Notes

The authors declare no competing financial interest.

ACKNOWLEDGMENTS

This research was supported by NSFC (No. 20903052, 20772054), the program for Liaoning excellent talents in University (LJQ 2011003), the innovative team project of education department of Liaoning Province (LT2011001), and Liaoning university support (2012LDGY06). A.F. acknowledges CINECA for the computational resources through a LISA 2013 Initiative (Laboratory for Interdisciplinary Advanced Simulation 2013) grant and CARIPLO for financial support (Project PLENOS). J.M.R. would like to thank the Istituto Italiano di Tecnologia for financial support.

REFERENCES

(1) Schmidt, G. M. H. *Pure Appl. Chem.* **1971**, *27*, 647−678.
(2) Tanaka, K.; Toda, F. *Chem. Rev.* **2000**, *100*, 1025−1074.
(3) Kawano, M.; Fujita, M. *Coord. Chem. Rev.* **2007**, *251*, 2592−2605.
(4) Kole, G. K.; Vittal, J. J. *Chem. Soc. Rev.* **2013**, *42*, 1755−1775.
(5) Biradha, K.; Santra, R. *Chem. Soc. Rev.* **2013**, *42*, 950−967.
(6) Espallargas, G. M.; Brammer, L.; van de Streek, J.; Shankland, K.; Florence, A. J.; Adams, H. *J. Am. Chem. Soc.* **2006**, *128*, 9584−9585.
(7) Metrangolo, P.; Carcenac, Y.; Lahtinen, M.; Pilati, T.; Rissanen, K.; Vij, A.; Resnati, G. *Science* **2009**, *323*, 1461−1464.
(8) Raatikainen, K.; Risanen, K. *Chem. Sci.* **2012**, *3*, 1235−1239.
(9) Coronado, E.; Giménez-Marqués, M.; Espallargas, G. M.; Brammer, L. *Nat. Commun.* **2012**, *3*, 828−836.
(10) Meazza, L.; Martí-Rujas, J.; Terraneo, G.; Castiglioni, C.; A. Milani, A.; Pilati, T.; Metrangolo, P.; Resnati, G. *CrystEngComm* **2011**, *13*, 4427−4435.
(11) Ohtsu, H.; Choi, W.; Islam, N.; Matsushita, Y.; Kawano, M. *J. Am. Chem. Soc.* **2013**, *135*, 11449−11452.
(12) Wenger, O. S. *Chem. Rev.* **2013**, *113*, 3686−3733.
(13) Naumov, P. *Top. Curr. Chem.* **2012**, *315*, 111−132.
(14) Caronna, T.; Liantonio, R.; Logothetis, T. A.; Metrangolo, P.; Pilati, T.; Resnati, G. *J. Am. Chem. Soc.* **2004**, *126*, 4500−4501.
(15) Guo, F.; Martí-Rujas, J.; Pan, Z.; Hughes, C. E.; Harris, K. D. M. *J. Phys. Chem. C* **2008**, *112*, 19793−19796.
(16) Kole, G. K.; Kojima, T.; Kawano, M. *Angew. Chem., Int. Ed.* **2014**, *53*, 2143−2146.
(17) Kissel, P.; Murray, D. J.; Wulftange, W. J.; Catalano, V. J.; King, B. T. *Nat. Chem.* **2014**, *6*, 774−778.
(18) Park, J.; Yuan, D.; Pham, K. T.; Li, J.-R.; Yakovenko, A.; Zhou, H.-C. *J. Am. Chem. Soc.* **2012**, *134*, 99−102.
(19) Pathigoolla, A.; Sureshan, K. M. *Angew. Chem., Int. Ed.* **2013**, *52*, 8671−8675.

(20) Fernández-Mato, A.; García, M. D.; Peinador, C.; Quintela, J. M.; Sánchez-Andújar, M.; Pato-Doldán, B.; Señarís-Rodríguez, M. A.; Tordera, D.; Bolink, H. J. *Cryst. Growth Des.* **2013**, *13*, 460−464.
(21) Martí-Rujas, J.; Meazza, L.; Lim, G. K.; Terraneo, G.; Pilati, T.; Harris, K. D. M.; Metrangolo, P.; Resnati, G. *Angew. Chem., Int. Ed.* **2013**, *52*, 13444−13448.
(22) Martí-Rujas, J.; Kawano, M. *Acc. Chem. Res.* **2013**, *46*, 493−505.
(23) Garay, A. L.; Pichon, A.; James, S. L. *Chem. Soc. Rev.* **2007**, *36*, 846−855.
(24) Sheldon, R. A. *Green Chem.* **2005**, *7*, 267−278.
(25) James, S. L.; Adams, C. J.; Bolm, C.; Braga, D.; Collier, P.; Friščić, T.; Grepioni, F.; Harris, K. D. M.; Hyett, G.; Jones, W.; Krebs, A.; Mack, J.; Maini, L.; Orpen, A. G.; Parkin, I. P.; Shearouse, W. C.; Steed, J. W.; Waddell, D. C. *Chem. Soc. Rev.* **2012**, *41*, 413−447.
(26) Guo, F.; Shao, H.; Yang, Q.; Famulari, A.; Martí-Rujas, J. *CrystEngComm* **2014**, *16*, 969−973.
(27) Friščić, T. *Chem. Soc. Rev.* **2012**, *41*, 3493−3510.
(28) Braga, D.; Grepioni, F.; Lampronti, G. I. *CrystEngComm* **2011**, *13*, 3122−3124.
(29) Lin, J.; Martí-Rujas, J.; Metrangolo, P.; Pilati, T.; Radice, S.; Resnati, G.; Terraneo, G. *Cryst. Growth Des.* **2012**, *12*, 5757−5762.
(30) Santra, R.; Biradha, K. *Cryst. Growth Des.* **2010**, *10*, 3315−3320.
(31) Užarević, K.; Rubčić, M.; Radić, M.; Puškarić, A.; Cindrić, M. *CrystEngComm* **2011**, *13*, 4314−4323.
(32) Adams, C. J.; Kurawa, M. A.; Orpen, A. G. *Inorg. Chem.* **2010**, *49*, 10475−10485.
(33) Friščić, T.; Fábián, L. *CrystEngComm* **2009**, *11*, 743−745.
(34) Wang, P.; Li, G.; Chen, Y.; Chen, S.; James, S. L.; Yuan, W. *CrystEngComm* **2012**, *14*, 1994−1997.
(35) Braga, D.; Grepioni, F.; Maini, L.; Mazzeo, P. P.; Ventura, B. *New J. Chem.* **2011**, *35*, 339−344.
(36) Ravnsbæk, J. B.; Swager, T. M. *ACS Macro Lett.* **2014**, *3*, 305−309.
(37) André, V. M.; Hardeman, A.; Halasz, I.; Stein, R. S.; Jackson, G. J.; Reid, D. G.; Duer, M. J.; Curfs, C.; Duarte, M. T.; Friščić, T. *Angew. Chem., Int. Ed.* **2011**, *50*, 7858−7861.
(38) Chow, E. H. H.; Strobridge, F. C.; Friščić, T. *Chem. Commun.* **2010**, *46*, 6368−6370.
(39) Braga, D.; Grepioni, F.; Maini, L.; Brescello, R.; Cotarca, L. *CrystEngComm* **2008**, *10*, 469−471.
(40) Beldon, P. J.; Fábián, L.; Stein, R. S.; Thirumurugan, A.; Cheetham, A. K.; Friščić, T. *Angew. Chem., Int. Ed.* **2010**, *49*, 9640−9643.
(41) Yuan, W.; O'Connor, J.; James, S. L. *CrystEngComm* **2010**, *12*, 3515−3517.
(42) Bennett, T. D.; Cao, S.; Tan, J. C.; Keen, D. A.; Bithell, E. G.; Beldon, P. J.; Friščić, T.; Cheetham, A. K. *J. Am. Chem. Soc.* **2011**, *133*, 14546−14549.
(43) Yuan, W.; Garay, A. L.; Pichon, A.; Clowes, R.; Wood, C. D.; Cooper, A. I.; James, S. L. *CrystEngComm* **2010**, *12*, 4063−4065.
(44) Friščić, T.; Halasz, I.; Beldon, P. J.; Belenquer, A. M.; Adams, F.; Kimber, S. A. J.; Honkimaki, V.; Dinebier, R. E. *Nat. Chem.* **2013**, *5*, 66−73.
(45) Karki, S.; Friščić, T.; Jones, W. *CrystEngComm* **2009**, *11*, 470−481.
(46) Braga, D.; Grepioni, F.; Lampronti, G. I. *CrystEngComm* **2011**, *13*, 3122−3124.
(47) Loots, L.; Wahl, H.; van der Westhuizen, L.; Haynes, D. A.; le Roex, T. *Chem. Commun.* **2012**, *48*, 11507−11509.
(48) Kaur, R.; Lalithalakshimi, B. V.; Guru Row, T. N. *Cryst. Growth Des.* **2014**, *14*, 2614−2620.
(49) LAG refers to mechanical reactions aided by the addition of stoichiometric amounts of solvent.
(50) Guo, F.; Zhang, M. Q.; Famulari, A.; Martí-Rujas, J. *CrystEngComm* **2013**, *15*, 6237−6243.
(51) Famulari, A.; Raos, G.; Baggioli, A.; Casalegno, M.; Po, R.; Meille, S. V. *J. Phys. Chem. B* **2012**, *116*, 14504−14509.
(52) Du, G.; Liu, Z.; Chu, Q.; Li, Z.; Zhang, S. *Acta Crystallogr.* **2008**, *E64*, o1947−o1948.
(53) The two hydrogens involved in the proton transfer can also be corroborated by the changes in the bond lengths of the functional groups involved in the interaction (i.e., C−O lengths of carboxyl, S−O lengths of sulfonate group and C−N lengths of B cation) (Supporting Information, Table S1).
(54) Smith, G.; Wermuth, U. D.; Healy, P. C. *Acta Crystallogr., Sect. E: Struct.* **2006**, *E62*, o1863−o1865.
(55) CSD code: SSALAD10.
(56) In fact, it has been shown that neat grinding of pamoic acid and DABCO in a 1:1 stoichiometry resulted in a physical mixture of the two starting components and only adding five drops of water yielded the molecular salt.
(57) Bond, A. D. *CrystEngComm* **2007**, *9*, 833−834.
(58) Zukerman-Schpector, J.; Tiekink, E. R. T. *Z. Kristallogr.* **2008**, *223*, 233−234.
(59) Steed, J. W. *Trends Pharmacol. Sci.* **2013**, *34*, 185−193.
(60) Wood, P. A.; Feeder, N.; Furlow, M.; Galek, P. T. A.; Groom, C. R.; Pidcock, E. *CrystEngComm* **2014**, *16*, 5839−5848.
(61) Karki, S.; Friščić, T.; Jones, W.; Motherwell, W. D. S. *Mol. Pharmaceutics* **2007**, *4*, 347−354.
(62) Sun, D.; Li, Y.-H.; Hao, H. J.; Liu, F. J.; Wen, Y. M.; Huang, R. B.; Zheng, L. S. *Cryst. Growth Des.* **2011**, *11*, 3323−3327.
(63) An anion is more polarizable because it has at least one extra electron which is generally allocated at higher energy levels. In this way it is easier to move this electron into the molecule. If we consider the energy levels of the system, easier to move means lower accessible energy levels for the electron suitable for absorption or emission of light (i.e., longer λ).
(64) Tretiak, S.; Mukamel, S. *Chem. Rev.* **2002**, *102*, 3171−3212.
(65) Ottonelli, M.; Musso, G.; Dellepiane, G. *J. Phys. Chem. A* **2008**, *112*, 3991−3995.
(66) Quarti, C.; Fazzi, D.; Tommasini, M. *A, Chem. Phys. Lett.* **2010**, *496*, 284−290.
(67) Nicolini, T.; Famulari, A.; Gatti, T.; Martí-Rujas, J.; Villafiorita Monteleone, F.; Canesi, E. V.; Meinardi, F.; Botta, C.; Parisini, E.; Meille, S. V.; Bertarelli, C. *J. Phys. Chem. Lett.* **2014**, *5*, 2171−2176.
(68) Frisch, M. J.; Trucks, G. W.; Schlegel, H. B.; Scuseria, G. E.; Robb, M. A.; Cheeseman, J. R.; Scalmani, G.; Barone, V.; Mennucci, B.; Petersson, G. A.; et al.. *Gaussian 09*, Revision A.1, Gaussian, Inc., Wallingford, CT, 2009.